The importance of thermal stresses and strains induced in laser processing with focused Gaussian beams

Cite as: Journal of Applied Physics **64**, 6274 (1988); https://doi.org/10.1063/1.342086
Submitted: 11 April 1988 • Accepted: 09 August 1988 • Published Online: 04 June 1998

Lisa P. Welsh, Judah A. Tuchman and Irving P. Herman

The importance of thermal stresses and strains induced in laser processing with focused Gaussian beams

Lisa P. Welsh, Judah A. Tuchman, and Irving P. Herman
Department of Applied Physics, Columbia University, New York, New York 10027

(Received 11 April 1988; accepted for publication 9 August 1988)

The thermoelastic equations are solved for laser heating of a semi-infinite elastic medium by a focused TEM_{00} Gaussian beam. Single integral expressions are derived for stresses and strains, which are analytically evaluated on axis at the surface and far from the laser-heated region (for a laser spot size $\gg$ absorption depth), and numerically evaluated for the example of laser heating of a silicon substrate. This analysis is extended to the case of laser heating of thin films on substrates. Use of these stress and strain profiles suggests that dislocations may form at the surface during high-temperature laser processing of silicon at scan speeds typically used in direct laser writing. Also the elastic strains induced during laser heating shift phonon frequencies from their thermal equilibrium values, thereby complicating the use of Raman scattering as an optical probe of temperature. This is shown to be particularly significant for laser heating of silicon thin films on fused silica substrates and not very important for laser processing of silicon substrates or silicon thin films on sapphire.

I. INTRODUCTION

In direct laser writing, focused beams are used to modify surfaces by chemical processes that lead to deposition, etching, and doping.[1] This is often accomplished by locally heating the substrate using a focused laser with a Gaussian profile in the presence of a suitable reactant. During the course of this surface modification, large thermoelastic stresses and strains may be induced, which can produce defects and leave behind built-in stresses in and near the modified area. These unintended effects can lead to serious consequences in performance, especially in microelectronics, where many important applications of laser writing have been investigated. Similar problems may also arise in annealing and recrystallization using focused lasers and electron beams. The importance of these stresses and strains induced during laser writing are addressed here for the first time. Single integral expressions for stresses and strains are derived for model systems using the coupled laser heating and thermoelastic equations. The consequences of these solutions are then analyzed using laser processing of a crystalline silicon substrate as an example.

Stresses induced in electron beam annealing of silicon by a scanning line focus have been analyzed by Correra and Bentini,[2] who later extended their study to uniform heating of the substrate.[3] They also determined the pattern of dislocation formation during annealing from their calculated stress and strain distributions. A similar treatment of defect production is performed here, using the stress profiles induced during laser heating by a Gaussian beam.

Large elastic strains can dramatically affect the accuracy of temperature measurements made by optical probing during laser processing. The influence of strain in the Raman microprobe analysis of substrate heating by focused laser beams is investigated in this study as another example of a thermoelastic effect which is important in laser processing. Jellison and Wood,[4] and Compaan, Lee, and Trott[5] have found that strain can be an important factor in the Raman measurement of temperature during pulsed laser annealing by large uniform-intensity beams.

Lax[6,7] has obtained the solution for the temperature profile induced by steady-state heating of a uniform substrate by a focused laser beam. This solution is used here within the driving terms of the thermoelastic equations, which are then solved using techniques similar to those used by Lax. In ways, this analysis parallels that followed in photothermal displacement spectroscopy.[8]

The solutions for laser-induced stresses and strains in a uniform substrate and in a thin film overlaying a substrate are examined in Sec. II. In Sec. III these solutions are applied to the problems of defect formation during laser processing and Raman analysis of laser heating. Conclusions are given in Sec. IV. The basic thermoelastic relations are presented in the Appendix.

II. ANALYSIS

A. Uniform substrate

A focused laser with beam waist w and power P_0 is incident on the surface of a semi-infinite elastic substrate ($z \geqslant 0$) with absorption coefficient α and thermal conductivity K, which are presently assumed to be independent of the temperature T_t. The incident laser intensity is assumed to be cylindrically symmetric:

$$I(r,z=0) = I_0 f(r/w), \qquad (1)$$

where

$$f(r/w) = \exp(-r^2/w^2), \qquad (2)$$

and $I_0 = P_0/(\pi w^2)$ for TEM_{00} mode Gaussian beams.

For steady-state conditions, the heat flow equation is

$$\nabla^2 T(r,z) = -\frac{\alpha(1-R_0)I_0}{K}\exp(-\alpha z) f(r/w), \quad (3)$$

where T is the temperature rise due to the laser ($T_t = T + T_{\text{ambient}}$), and R_0 is the surface reflectivity. Lax[6] has solved Eq. (3) using the normalized coordinates:

$$R = r/w, \quad Z = z/w, \quad W = \alpha w, \tag{4}$$

obtaining

$$T(R,Z,W) = \overline{T}\int_0^\infty J_0(\lambda R)F(\lambda) \times \frac{W\exp(-\lambda Z) - \lambda\exp(-WZ)}{W^2 - \lambda^2}\,d\lambda, \tag{5}$$

where

$$\overline{T} = \alpha P_0(1 - R_0)/\pi K, \tag{6}$$

and $F(\lambda)$ is the Bessel transform of $f(R)$:

$$F(\lambda) = \int_0^\infty f(R)J_0(\lambda R)R\,dR, \tag{7}$$

with

$$F(\lambda) = \tfrac{1}{2}\exp(-\tfrac{1}{4}\lambda^2), \tag{8}$$

for the Gaussian beam described by Eq. (2). At $R = 0$, $Z = 0$, the temperature rise is $T = T_{\max}$ in the limit $w \gg 1/\alpha$ ($W \to \infty$), where

$$T_{\max} = T(R = 0, Z = 0, W = \infty) = \frac{\sqrt{\pi}}{2W}\overline{T} = \frac{P_0(1 - R_0)}{2\sqrt{\pi}Kw}. \tag{9}$$

This laser-heated temperature profile leads to thermoelastic stresses and strains in the substrate. The Appendix gives the relations between the induced residual stresses σ, strains ϵ, and displacements u for an isotropic solid. ϵ is the total strain, which is the sum of the elastic strain $\overline{\epsilon}$ and the strain from thermal expansion. For diagonal components this amounts to

$$\epsilon = \overline{\epsilon} + \alpha' T, \tag{10}$$

while for off-diagonal elements $\epsilon = \overline{\epsilon}$. α' is the coefficient of thermal expansion.

The relations for stresses and strains in the Appendix may be combined and then expressed in terms of Youngdahl stress functions[9] Ω and Ψ to give

$$\nabla^2\Omega = \frac{1}{2(1-\nu)}\left(-\frac{\partial^2\Psi}{\partial Z^2} + 2(1+\nu)w^2\alpha' T\right), \tag{11}$$

$$\nabla^2\Psi = 0, \tag{12}$$

which are Eqs. (A6) and (A7) in the Appendix expressed in the normalized coordinates of Eq. (4). ν is Poisson's ratio. Equations (A4) and (A5) relate the displacement u and strain ϵ to Ω and Ψ, and Eqs. (A1) relate the stress σ to ϵ. Because the laser heating is axisymmetric and the material is isotropic, the solution is most easily expressed in cylindrical coordinates and is independent of θ.

The solution to the homogeneous Eq. (12) is

$$\Psi = \Omega_0\int_0^\infty J_0(\lambda R)\exp(-\lambda Z)P(\lambda)d\lambda, \tag{13}$$

and the homogeneous solution to Eq. (11) is

$$\Omega_{\text{hom}} = \Omega_0\int_0^\infty J_0(\lambda R)\exp(-\lambda Z)H(\lambda)d\lambda, \tag{14}$$

where Ω_0 has been set equal to $[(1+\nu)/(1-\nu)]w^2\alpha'\overline{T}$ for later convenience, and $P(\lambda)$ and $H(\lambda)$ need to be determined.

The complete solution to Eq. (11) is

$$\Omega = \Omega_{\text{hom}} - \Omega_0\int_0^\infty J_0(\lambda R)F(\lambda)\frac{\lambda\exp(-WZ)}{(W^2-\lambda^2)^2}d\lambda - \frac{\Omega_0 W}{2}\int_0^\infty J_0(\lambda R)F(\lambda)\frac{Z\exp(-\lambda Z)}{\lambda(W^2-\lambda^2)}d\lambda + \frac{\Omega_0 Z}{4(1-\nu)}\int_0^\infty J_0(\lambda R)P(\lambda)\lambda\exp(-\lambda Z)d\lambda, \tag{15}$$

where the second and third terms on the right-hand side are the particular solutions for the temperature term of Eq. (11), and the fourth term is the particular solution for the $\partial^2\Psi/\partial Z^2$ term.

$P(\lambda)$ and $H(\lambda)$ are determined from the boundary conditions for the stress-free surface, $\sigma_{zz}(R,Z=0) = \sigma_{rz}(R,Z=0) = 0$. Using the relations between the stresses and stress functions obtainable from Eqs. (A1) and (A5) in the Appendix, the following conditions are obtained:

$$2\lambda H(\lambda) + \frac{W(W^2-3\lambda^2)}{\lambda(W^2-\lambda^2)^2}F(\lambda) + \lambda\frac{1-2\nu}{2(1-\nu)}P(\lambda) = 0, \tag{16a}$$

$$H(\lambda) - \frac{\lambda}{(W^2-\lambda^2)^2}F(\lambda) + \frac{1}{2}P(\lambda) = 0. \tag{16b}$$

These are solved to yield

$$P(\lambda) = 2\frac{B(\lambda) - A(\lambda)}{\lambda^2}F(\lambda), \tag{17}$$

$$H(\lambda) = \frac{A(\lambda)}{\lambda^2}F(\lambda), \tag{18}$$

where $F(\lambda)$ is the Bessel transform of the laser profile given by Eq. (7) in general and by Eq. (8) for a Gaussian beam. To simplify these expressions, the functions $A(\lambda)$ and $B(\lambda)$ have been introduced here, which, along with the function $C(\lambda)$, are used below in the integral expressions for stresses and strains. These are defined as

$$A(\lambda) = \frac{\lambda^3 - (W+2\lambda)(1-\nu)(W-\lambda)^2}{(W^2-\lambda^2)^2}, \tag{19}$$

$$B(\lambda) = \frac{\lambda^3}{(W^2-\lambda^2)^2}, \tag{20}$$

$$C(\lambda) = \frac{\lambda^3}{(W+\lambda)(W^2-\lambda^2)}. \tag{21}$$

[Despite the close connection between $B(\lambda)$ and $C(\lambda)$, it is still convenient to use both functions.]

In terms of $F(\lambda)$ the stress functions are then

$$\Omega = \Omega_0\int_0^\infty \frac{J_0(\lambda R)F(\lambda)}{\lambda^2}[A(\lambda)\exp(-\lambda Z) - B(\lambda) \times\exp(-WZ) - C(\lambda)Z\exp(-\lambda Z)]d\lambda, \tag{22}$$

$$\Psi = 2\Omega_0\int_0^\infty \frac{J_0(\lambda R)F(\lambda)}{\lambda^2} \times[B(\lambda) - A(\lambda)]\exp(-\lambda Z)d\lambda. \tag{23}$$

Using the relations in the Appendix, expressions for the

TABLE I. Integral expressions for stresses, total strains, and displacements.

Stresses

$$\sigma_{rr} = -\sigma_0 \int_0^\infty J_0(\lambda R) F(\lambda) \left[\left(\frac{2W}{\lambda} - 1 \right) B(\lambda) \exp(-\lambda Z) - \frac{W^2}{\lambda^2} B(\lambda) \exp(-WZ) - C(\lambda) Z \exp(-\lambda Z) \right] d\lambda$$

$$+ \sigma_0 \int_0^\infty \frac{J_1(\lambda R)}{\lambda R} F(\lambda) [A(\lambda) \exp(-\lambda Z) - B(\lambda) \exp(-WZ) - C(\lambda) Z \exp(-\lambda Z)] d\lambda$$

$$\sigma_{\theta\theta} = \sigma_0 \int_0^\infty J_0(\lambda R) F(\lambda) \left\{ \left[A(\lambda) + B(\lambda) \left(1 - \frac{2W}{\lambda} \right) \right] \exp(-\lambda Z) + \frac{W^2 - \lambda^2}{\lambda^2} B(\lambda) \exp(-WZ) \right\} d\lambda$$

$$- \sigma_0 \int_0^\infty \frac{J_1(\lambda R)}{\lambda R} F(\lambda) [A(\lambda) \exp(-\lambda Z) - B(\lambda) \exp(-WZ) - C(\lambda) Z \exp(-\lambda Z)] d\lambda$$

$$\sigma_{zz} = \sigma_0 \int_0^\infty J_0(\lambda R) F(\lambda) \{ B(\lambda) [\exp(-\lambda Z) - \exp(-WZ)] - C(\lambda) Z \exp(-\lambda Z) \} d\lambda$$

$$\sigma_{rz} = -\sigma_0 \int_0^\infty J_1(\lambda R) F(\lambda) \left(\frac{W}{\lambda} B(\lambda) [\exp(-\lambda Z) - \exp(-WZ)] - C(\lambda) Z \exp(-\lambda Z) \right) d\lambda$$

Total strains

$$\epsilon_{rr} = -\epsilon_0 \int_0^\infty \left(J_0(\lambda R) - \frac{J_1(\lambda R)}{\lambda R} \right) F(\lambda) [A(\lambda) \exp(-\lambda Z) - B(\lambda) \exp(-WZ) - C(\lambda) Z \exp(-\lambda Z)] d\lambda$$

$$\epsilon_{\theta\theta} = -\epsilon_0 \int_0^\infty \frac{J_1(\lambda R)}{\lambda R} F(\lambda) [A(\lambda) \exp(-\lambda Z) - B(\lambda) \exp(-WZ) - C(\lambda) Z \exp(-\lambda Z)] d\lambda$$

$$\epsilon_{zz} = \epsilon_0 \int_0^\infty J_0(\lambda R) F(\lambda) \left[\left(\frac{2W}{\lambda} B(\lambda) - A(\lambda) \right) \exp(-\lambda Z) - \frac{W^2}{\lambda^2} B(\lambda) \exp(-WZ) - C(\lambda) Z \exp(-\lambda Z) \right] d\lambda$$

$$\epsilon_{rz} = -2\epsilon_0 \int_0^\infty J_1(\lambda R) F(\lambda) \left(\frac{W}{\lambda} B(\lambda) [\exp(-\lambda Z) - \exp(-WZ)] - C(\lambda) Z \exp(-\lambda Z) \right) d\lambda$$

Displacements

$$u_r = -w\epsilon_0 \int_0^\infty \frac{J_1(\lambda R)}{\lambda} F(\lambda) [A(\lambda) \exp(-\lambda Z) - B(\lambda) \exp(-WZ) - C(\lambda) Z \exp(-\lambda Z)] d\lambda$$

$$u_z = -w\epsilon_0 \int_0^\infty \frac{J_0(\lambda R)}{\lambda} F(\lambda) \left\{ \left[B(\lambda) \left(1 + \frac{W}{\lambda} \right) - A(\lambda) \right] \exp(-\lambda Z) - \frac{W}{\lambda} B(\lambda) \exp(-WZ) - C(\lambda) Z \exp(\lambda Z) \right\} d\lambda$$

stresses and strains are derived easily and are tabulated in Table I in terms of σ_0 and ϵ_0, respectively, where

$$\epsilon_0 = \frac{\Omega_0}{w^2} = \frac{1+\nu}{1-\nu} \frac{2\alpha' W}{\sqrt{\pi}} T_{\max}, \tag{24}$$

$$\sigma_0 = \frac{E}{1+\nu} \epsilon_0, \tag{25}$$

and E is Young's modulus.

As shown by Lax,[6] the highest temperature rise for Gaussian beam heating is attained at $R=0$, $Z=0$, and is greatest for $W \to \infty$. $T_{\max} = T(R=0, Z=0, W=\infty)$, as given in Eq. (9), is a useful reference for normalizing temperature rises for $R \neq 0$, $Z \neq 0$, and finite W.

Similarly, the maximum stresses and strains occur at $R=0$, $Z=0$, and again these are largest as $W \to \infty$. From Table I, for $W \to \infty$,

$$\sigma_{rr}(R=0, Z=0) = \sigma_{\theta\theta}(0,0) = \sigma_{\max} = -\frac{E\alpha'}{2} T_{\max}, \tag{26}$$

where

$$\sigma_{\max} = -(1-\nu) \frac{\sqrt{\pi}}{4W} \sigma_0.$$

Also

$$\epsilon_{zz}(R=0, Z=0) = \epsilon_{\max} = (1+\nu)\alpha' T_{\max}, \tag{27a}$$

$$\epsilon_{rr}(R=0, Z=0) = \epsilon_{\theta\theta}(0,0) = \frac{\epsilon_{\max}}{2} = \frac{(1+\nu)}{2} \alpha' T_{\max}, \tag{27b}$$

where $\epsilon_{\max} = (1-\nu)(\sqrt{\pi}/2W)\epsilon_0$. Note that $\epsilon_{rr}(R=0, Z) = \epsilon_{\theta\theta}(R=0, Z)$, but $\epsilon_{rr} \neq \epsilon_{\theta\theta}$ away from the axis of symmetry.

Using Eq. (10), the elastic strains at the origin in the limit $W \to \infty$ are

$$\bar{\epsilon}_{zz}(0,0) = \nu\alpha' T_{\max}, \tag{28a}$$

$$\bar{\epsilon}_{rr}(0,0) = \bar{\epsilon}_{\theta\theta}(0,0) = \frac{\nu - 1}{2} \alpha' T_{\max}. \tag{28b}$$

The expressions for stresses and strains in Table I have been integrated for R and/or $Z \gg 1$ (r and/or $z \gg w$) in the limit $W \to \infty$, and are presented in Table II. For comparison, note that the temperature rise decays as $1/\sqrt{r^2+z^2}$ for large r and/or z.[6] The rr and $\theta\theta$ stress components and the three diagonal total strain elements all decrease as the inverse of the characteristic distance from the origin, although only ϵ_{zz} decreases in the simple manner of the temperature rise. Furthermore, the rr and $\theta\theta$ components are related by

$$\epsilon_{rr} = \frac{z}{\sqrt{r^2+z^2}} \epsilon_{\theta\theta}$$

and

TABLE II. Limiting expressions for stresses and strains for $r \gg w$ and/or $z \gg w$ in the limit $W = \alpha w \to \infty$.

Stresses

$$\sigma_{rr} = \frac{w}{r^2}(\sqrt{r^2+z^2} - z)\frac{2\sigma_{max}}{\sqrt{\pi}}$$

$$\sigma_{\theta\theta} = \frac{z}{\sqrt{r^2+z^2}}\frac{w}{r^2}(\sqrt{r^2+z^2} - z)\frac{2\sigma_{max}}{\sqrt{\pi}}$$

$$\sigma_{zz} = -\frac{3}{1-\nu}\frac{wz^2}{\alpha^2}\left(\frac{3}{(r^2+z^2)^{5/2}} - \frac{5z^2}{(r^2+z^2)^{7/2}}\right)\frac{2\sigma_{max}}{\sqrt{\pi}}$$

$$\sigma_{rz} = \frac{3}{1-\nu}\frac{w}{\alpha^2}\frac{z}{r}\left(\frac{2}{(r^2+z^2)^{3/2}} - \frac{7z^2}{(r^2+z^2)^{5/2}} + \frac{5z^4}{(r^2+z^2)^{7/2}}\right)\frac{2\sigma_{max}}{\sqrt{\pi}}$$

Total strains

$$\epsilon_{rr} = \frac{z}{\sqrt{r^2+z^2}}\frac{w}{r^2}(\sqrt{r^2+z^2} - z)\frac{\epsilon_{max}}{\sqrt{\pi}}$$

$$\epsilon_{\theta\theta} = \frac{w}{r^2}(\sqrt{r^2+z^2} - z)\frac{\epsilon_{max}}{\sqrt{\pi}}$$

$$\epsilon_{zz} = \frac{w}{\sqrt{r^2+z^2}}\frac{\epsilon_{max}}{\sqrt{\pi}}$$

$$\epsilon_{rz} = -\frac{6}{1-\nu}\frac{w}{\alpha^2}\frac{z}{r}\left(\frac{2}{(r^2+z^2)^{3/2}} - \frac{7z^2}{(r^2+z^2)^{5/2}} + \frac{5z^4}{(r^2+z^2)^{7/2}}\right)\frac{\epsilon_{max}}{\sqrt{\pi}}$$

$$\sigma_{\theta\theta} = \frac{z}{\sqrt{r^2+z^2}}\sigma_{rr}.$$

Also, $\epsilon_{zz} = \epsilon_{rr} + \epsilon_{\theta\theta}$. In fact, this relation is true for all r and z in the $W \to \infty$ limit. σ_{zz}, σ_{rz}, and ϵ_{rz} are much smaller than these other components because the absorption coefficient α is very large in this assumed limit. They also decrease much more rapidly with the characteristic distance from the origin, as the inverse of the third power.

The solutions represented by Eqs. (22) and (23), and Tables I and II assume that the laser heating parameters α, R_0, and K used in Eq. (3), and the thermoelastic parameters ν, α', and E in Eqs. (11) and (12), and the Appendix, are all independent of temperature and strain. This is usually a good approximation for the thermoelastic parameters. For example, in silicon C_{11}, C_{12}, and C_{44} (related to ν and E in the Appendix) vary by only $\sim 10\%$ from $T = 300$–1690 K.[10] They are also fairly independent of strain in the regimes of interest.[11] Furthermore, changes in the coefficients of thermal expansion α' are usually small.[12] For example, they vary by only about $\pm 20\%$ in silicon, sapphire, and fused silica within the temperature range of interest.

While the surface reflectivity R_0 also usually varies slowly with temperature, the other laser heating parameters more often vary fairly strongly with temperature. The absorption coefficient α varies rapidly with T_t for many materials, including silicon.[13] However, the sensitive parameter of interest in the analysis is not α but $W = \alpha w$. When $W \gg 1$, the temperature profile is independent of α. For $W \lesssim 1$, the variations in $\alpha(T_t)$ may be of significance. Variations of the thermal conductivity K with temperature may be large and can affect T, and therefore also σ and ϵ, quite strongly. For example, in silicon K decreases from 1.5 to 0.2 W/cm degree from $T_t = 300$–1690 K.[14]

Lax[7] has shown that the temperature rise profile given by Eq. (5) (which assumes constant thermal conductivity) is in fact the solution for the Kirchoff-transformed temperature Θ in cases where the thermal conductivity is temperature dependent. The temperature rise T is then obtained from Θ by an inverse Kirchoff transformation. Unfortunately, there is no longer an obvious analytic solution to the thermoelastic equations [Eqs. (11) and (12)] when T is substituted after the transformation if the thermal conductivity depends on temperature. Still, in cases with temperature-dependent thermal conductivity an approximate solution for stresses and strains may be obtained by solving for T exactly using $K(T_t)$, and then finding constant parameters K and α (and also P_0, w, etc.) which will nearly simulate the actual temperature profile. To first order, this can be done by adjusting P_0 and K to match the maximum temperature rise at $r = 0$, $z = 0$, which amounts to using T_{max}, defined in Eq. (9), as a parameter. The thermoelastic equations can then be solved as described previously. This approach is adopted here in the examples that follow.

The analytic stress and strain expressions in Table I are now examined for a Gaussian beam. Thermoelastic constants for silicon are used in these examples because of the importance of this semiconductor in microelectronics and the frequent use of lasers in processing silicon. ($\alpha' = 4.0 \times 10^{-6}$/°C, $\nu = 0.42$, $E = 1.13 \times 10^{12}$ dyn/cm^2.[12]) Since this analysis assumes an isotropic solid, while silicon has higher order, cubic symmetry, application to silicon is only approximately correct. Reference 2 estimates that the accuracy of results from isotropic thermoelastic analysis to silicon is better than 20%. Assumption of cubic symmetry in thermoelastic analysis makes solution significantly more difficult.

Using Eqs. (9), (26), and (27), the maximum stresses and strains induced in heating silicon to $T = T_{max} = 1400$ °C ($T_t = 1420$ °C $\cong T_{melt}$) can be found in the $W = \alpha w \to \infty$ limit. The maximum residual stress is $\sigma_{max} = \sigma_{rr} = \sigma_{\theta\theta} = -3.2 \times 10^9$ dyn/cm^2. The maximum total strains are $\epsilon_{zz} = 7.9 \times 10^{-3}$ and $\epsilon_{rr} = \epsilon_{\theta\theta} = 4.0 \times 10^{-3}$, while the maximum elastic strains are $\bar{\epsilon}_{zz} = 2.3 \times 10^{-3}$ and $\bar{\epsilon}_{rr} = \bar{\epsilon}_{\theta\theta} = -1.6 \times 10^{-3}$. Whereas the total strain is positive for all diagonal components, only the elastic strain $\bar{\epsilon}_{zz}$ is positive, while $\bar{\epsilon}_{rr}$ and $\bar{\epsilon}_{\theta\theta}$ are negative.

The expressions for stresses and total strains in Table I have been integrated numerically for a beam radius of 1 μm and $W = 15$, and are displayed in Figs. 2 and 3. These calculations approximate the $W \to \infty$ limit. P_0/K is chosen so that T_{max} equals 1400 °C. For reference, Fig. 1(a) plots $T(r,z)$ vs r at different depths z. $T(r = 0, z = 0) = 1300$ °C is somewhat less than T_{max} because W is only 15. These curves are similar to those given by Lax.[6] Using Eq. (10) and the data from Figs. 1(a) and 3, the elastic strains were computed, and are plotted in Fig. 4.

Figure 2 shows that the stress components σ_{rr} and $\sigma_{\theta\theta}$ are the largest. For $W = 15$ they peak at $r = 0$ and $z = 0$ to a value slightly smaller than the corresponding stress σ_{max} in the $W \to \infty$ limit. Both stresses decrease monotonically with increasing r and z, although σ_{rr} does so much more slowly than does $\sigma_{\theta\theta}$, for increasing r. This is expected from the

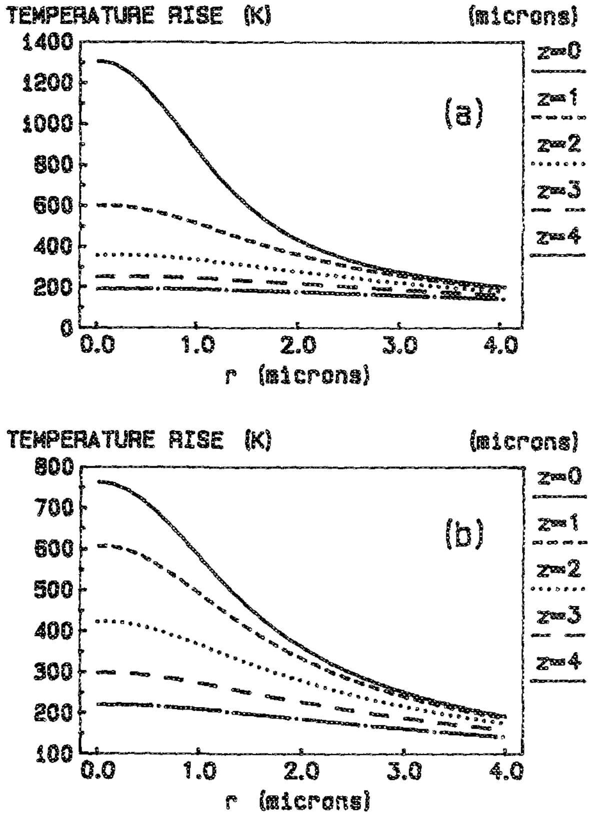

FIG. 1. Temperature rise (T) profiles vs r at $z = 0$, 1, 2, 3, and 4 μm, calculated from Eq. (5) using a spot size $w = 1$ μm and $T_{max} = 1400$ K: (a) $W = 15$ and (b) $W = 1$.

integrated expressions in Table II. σ_{zz} is smaller by about two orders of magnitude, peaking on axis at a depth of about 0.5 μm (not shown). σ_{rz} is also smaller than σ_{rr} and $\sigma_{\theta\theta}$ by about two orders of magnitude, and its magnitude peaks 0.8 μm off axis at a depth of about 0.1 μm. Near the axis, σ_{rz} is negative from the surface down to a depth of 0.6 μm, about zero at $z = 0.6$ μm, and positive deeper within the substrate. Because of the stated boundary conditions, both σ_{zz} and σ_{rz} are zero on the surface.

The total strains are displayed in Fig. 3. All three diagonal components are comparable in magnitude in this case. As predicted by the expressions given in Table II, the three strains decrease monotonically with r and z, but $\epsilon_{\theta\theta}$ (and also ϵ_{zz}) decreases much more slowly with r than does ϵ_{rr}, in contrast to the radial dependence of the corresponding stress components σ_{rr} and $\sigma_{\theta\theta}$. Again, these three major strain components peak at $r = 0$ and $z = 0$ to values somewhat smaller than those in the $W \rightarrow \infty$ limit. ϵ_{rz} is two orders of magnitude smaller than the diagonal components and varies as does σ_{rz}, which is expected since they are proportional to each other [Eq. (A1d)].

At $r = 0$ and $z = 0$ the elastic strains for $W = 15$, shown in Fig. 4, have nearly the same values as for the $W \rightarrow \infty$ limit, with $\bar{\epsilon}_{zz}$ positive and $\bar{\epsilon}_{rr}$ and $\bar{\epsilon}_{\theta\theta}$ both negative. However, in contrast to the total strain, the magnitude of $\bar{\epsilon}_{rr}$ reaches a maximum near a radius of $r = 1.4$ μm at the surface ($z = 0$). Also, $\bar{\epsilon}_{\theta\theta}$ changes sign to become positive at about the same radial distance for $z = 0$. Qualitatively similar behavior is observed below the surface ($z \geqslant 0$) (not shown).

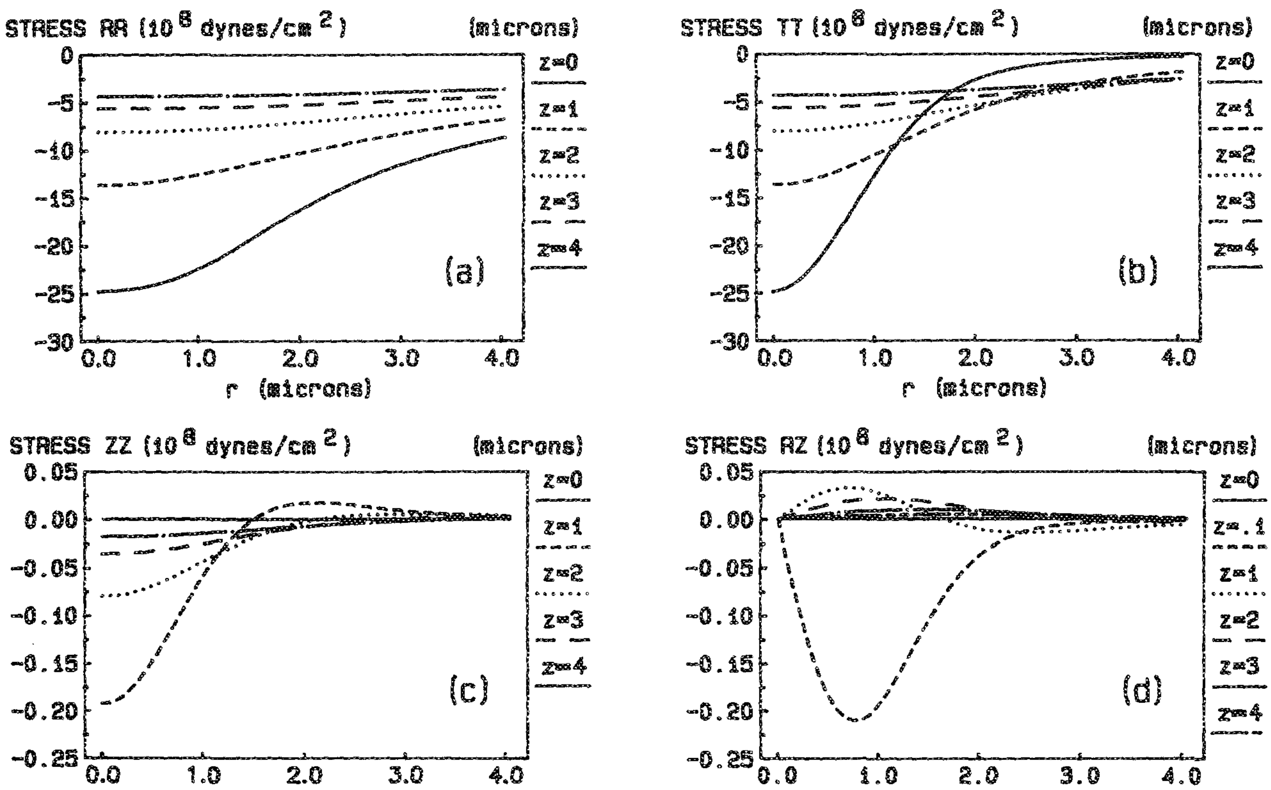

FIG. 2. Residual stresses vs r for $z = 0$–4 μm in silicon, calculated from Table I using $w = 1$ μm and $T_{max} = 1400$ K for $W = 15$: (a) σ_{rr}, (b) $\sigma_{\theta\theta}$, (c) σ_{zz}, and (d) σ_{rz}. In (d) $z = 0.1$ μm data are plotted, in addition to the $z = 0$, 1, 2, 3, and 4 μm data plotted for (a)–(c).

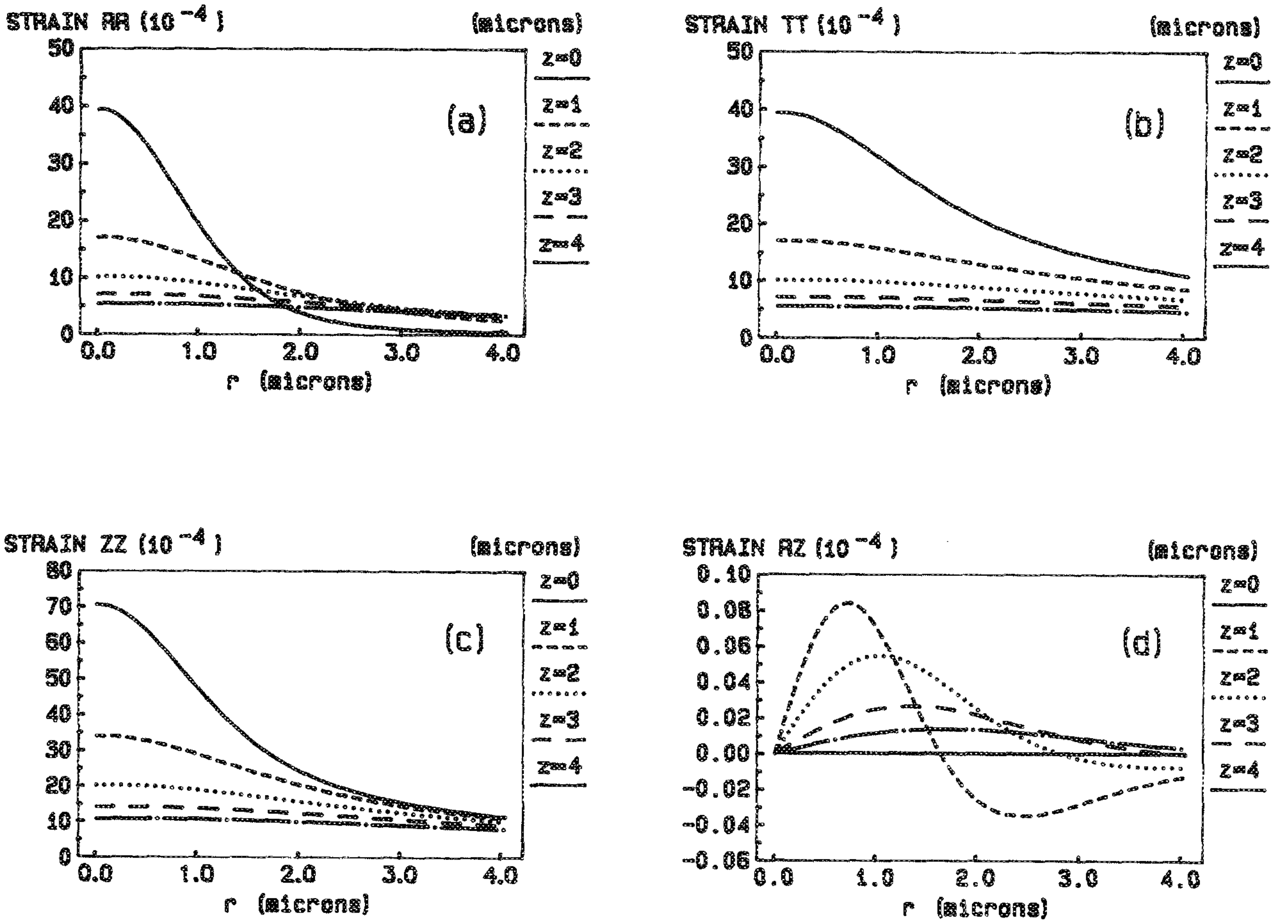

FIG. 3. Total strains vs r for $z = 0$–$4\,\mu$m in silicon calculated from Table I using $w = 1\,\mu$m and $T_{max} = 1400$ K for $W = 15$: (a) ϵ_{rr}, (b) $\epsilon_{\theta\theta}$, (c) ϵ_{zz}, and (d) ϵ_{rz}. The dependence of ϵ_{rz} vs r at $z = 0.1\,\mu$m may be determined from that of σ_{rz} in Fig. 2(d) since ϵ_{rz} and σ_{rz} are proportional.

Analogous calculations were performed for the $W = 1$ case in which the spot size w and the absorption depth $1/\alpha$ are equal (Figs. 5 and 6). For the same parameter $T_{max} = 1400$ K, the surface is significantly cooler with this condition vis-à-vis the large W limit, as shown in Fig. 1(b); at $r = 0$ and $z = 0$ the temperature rise is 760 K, significantly smaller than the 1300-K value for $W = 15$. Beneath the surface ($z \geqslant 1\,\mu$m), the $W = 1$ and 15 profiles are nearly the same. This agrees with the results in Ref. 6.

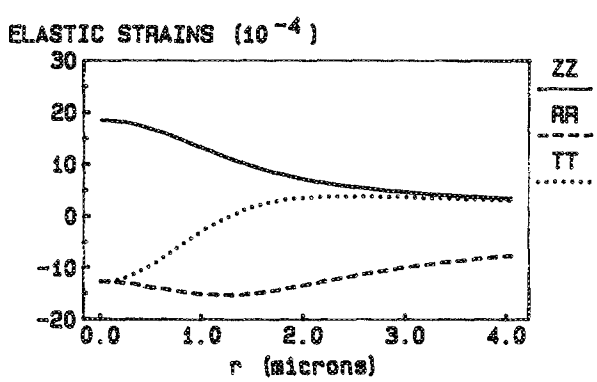

FIG. 4. Elastic strains ($\bar{\epsilon}_{zz}, \bar{\epsilon}_{rr}, \bar{\epsilon}_{\theta\theta}$) vs r in silicon at the surface ($z = 0\,\mu$m) computed from Figs. 1 and 3.

For $W = 1$, σ_{rr} and $\sigma_{\theta\theta}$ are similar, although somewhat smaller, than for $W = 15$, except at the surface where they dip to nearly zero at $r = 0$ and $z = 0$ (Fig. 5). Now σ_{zz} and σ_{rz} are relatively much larger than before, with σ_{zz} on the same order of magnitude and σ_{rz}, only one order smaller than σ_{rr} and $\sigma_{\theta\theta}$.

The diagonal components of the total strain are qualitatively the same for $W = 1$ and 15 (Fig. 6). For $W = 1$, ϵ_{rr} and $\epsilon_{\theta\theta}$ are slightly smaller, while ϵ_{zz} at the surface is significantly smaller. Also, ϵ_{rz} is now only one order of magnitude smaller than the diagonal components.

B. Thin film on a substrate

The above solution for thermoelastic stresses and strains can be extended to focused laser heating of a thin film on a substrate. Formally, this may be accomplished analytically by extending the Lax treatment of laser heating, as done by Calder and Sue[15] and Yamada, Nambu, and Yamamoto.[16] Then the thermoelastic equations can be solved in each of the two media with the boundary conditions that the stresses σ_{rz} and σ_{zz} are zero at the gas/film interface and the strains ϵ_{rr}

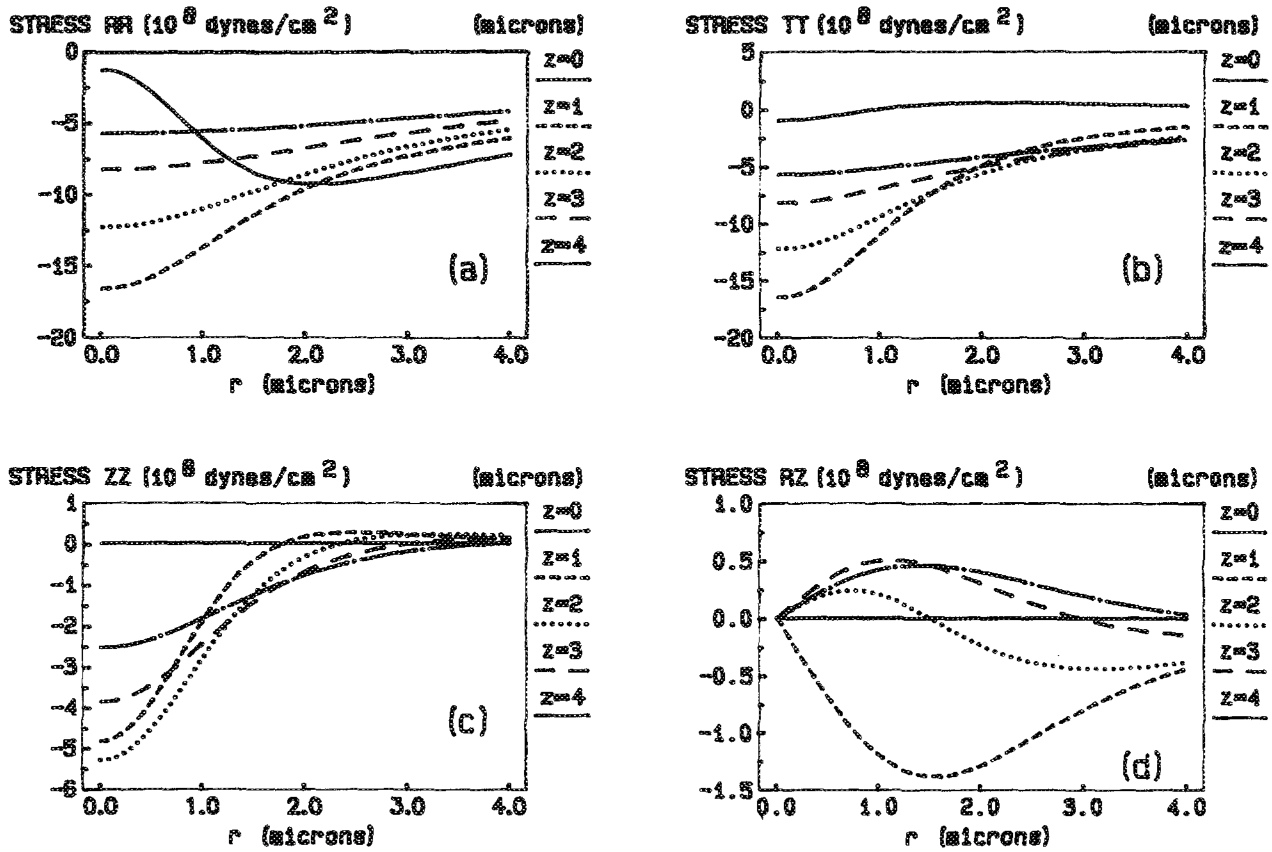

FIG. 5. Residual stresses in silicon as in Fig. 2, except $W = 1$.

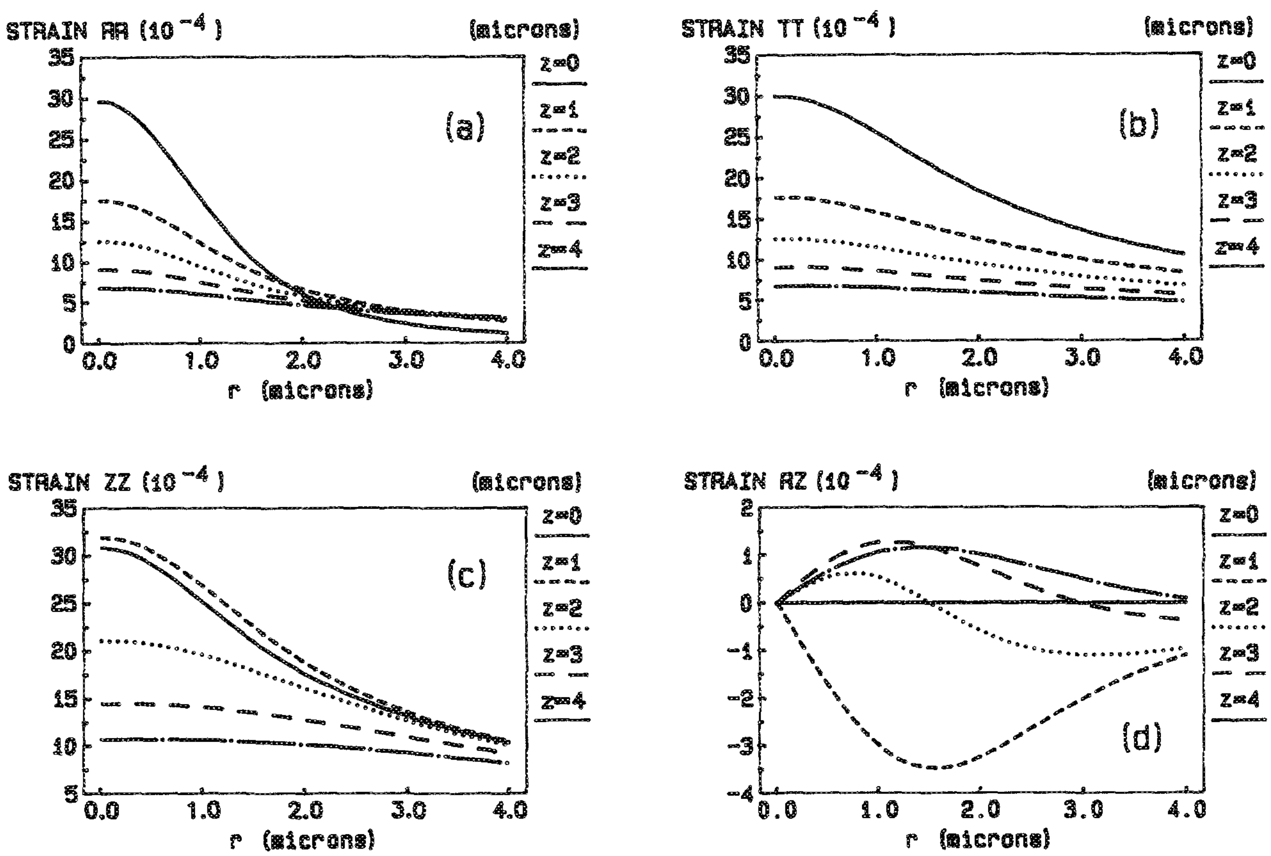

FIG. 6. Total strains in silicon as in Fig. 3, except $W = 1$.

and $\epsilon_{\theta\theta}$ are continuous from the substrate to the film. In the substrate, the general solution for the stress functions would be similar to Eqs. (13) and (15). Within the film the solution would be similar; however, expressions with exponential terms in these equations would be replaced by similar expressions with cosh and sinh terms, as in Ref. 8.

Instead of proceeding with this solution, which is complex for the general problem, only the important limiting case of a very thin film on an elastic substrate is considered here. The film is assumed to be thin enough that it does not perturb the stresses and strains in the substrate. This assumption is commonly made in analyzing stresses that are formed as a result of thin-film processing. Equation (5) still describes the temperature profile in the substrate in two limiting regimes. If only the thin film absorbs the laser, as for Si films on sapphire or SiO_2 substrates, Eq. (5) may be used in the $W\to\infty$ limit with P_0 replaced by $P_0[1-\exp(-\alpha_{\rm film}d)]$, where $\alpha_{\rm film}$ is the absorption coefficient of the film with thickness d ($\ll w$). In essence, laser absorption in the film is treated as absorption at the substrate surface with $\alpha_{\rm substrate}\to\infty$. If only the substrate absorbs the laser, as for SiO_2 films on Si, Eq. (5) is used unchanged. In both cases, thermal conduction in the thin film is assumed to be negligible compared to that through the substrate. Also, laser reflectivity at the gas/film and film/substrate interfaces, possibly including multiple reflections, must be considered properly. In either case, stresses and strains in the substrate would be determined from T using Eqs. (22) and (23) as above.

If both the film and substrate absorb the laser (and $\alpha_{\rm film}d\lesssim 1$), Eqs. (11) and (12) can be solved individually for thermoelastic effects that develop from T due to either heating source. However, $P_0\exp(-\alpha_{\rm film}d)$ (and not P_0) is used for the laser power in the term describing laser absorption within the substrate to account for laser attenuation in the film. The resulting σ and ϵ are then obtained by adding the individual stresses and strains resulting from heating the film or the substrate. This approach assumes the linearity of the laser heating and thermoelasticity equations, which is true only if all material parameters are independent of temperature and strain.

It is now assumed that the residual stresses σ^s and total strains ϵ^s in the substrate have been obtained as outlined above. Built-in strains and stresses at the film/substrate interface are assumed to be zero with no laser irradiation ($T=0$). Then the continuity of planar total strains gives the total strains in the film ϵ^f:

$$\epsilon^f_{rr}(r)=\epsilon^s_{rr}(r,z=0), \tag{29a}$$

$$\epsilon^f_{\theta\theta}(r)=\epsilon^s_{\theta\theta}(r,z=0), \tag{29b}$$

where from now on the actual coordinates r and z will be used instead of the normalized coordinates R and Z. Since the film is very thin, all components of ϵ^f do not vary with z within the film. Using Eq. (10), the elastic strains in the thin film, which describe the local deviation from thermal equilibrium (for unstressed film material), are

$$\bar{\epsilon}^f_{rr}(r)=\epsilon^s_{rr}(r,z=0)-\alpha'^{(f)}T(r,z=0), \tag{30a}$$

$$\bar{\epsilon}^f_{\theta\theta}(r)=\epsilon^s_{\theta\theta}(r,z=0)-\alpha'^{(f)}T(r,z=0), \tag{30b}$$

where $\alpha'^{(f)}$ is the coefficient of thermal expansion in the film.

Film strain in the z direction is obtained by setting $\sigma^f_{zz}(r)=0$ in Eq. (A1c), giving

$$\epsilon^f_{zz}(r)=\frac{\nu^{(f)}}{\nu^{(f)}-1}\left[\epsilon^f_{rr}(r)+\epsilon^f_{\theta\theta}(r)\right]+\frac{1+\nu^{(f)}}{1-\nu^{(f)}}\alpha'^{(f)}T(r,z=0), \tag{31}$$

$$\bar{\epsilon}^f_{zz}(r)=\frac{\nu^{(f)}}{\nu^{(f)}-1}\left[\bar{\epsilon}^f_{rr}(r)+\bar{\epsilon}^f_{\theta\theta}(r)\right], \tag{32}$$

and using Eqs. (30),

$$\bar{\epsilon}^f_{zz}(r)=\frac{\nu^{(f)}}{\nu^{(f)}-1}\left[\epsilon^s_{rr}(r,z=0)+\epsilon^s_{\theta\theta}(r,z=0)\right]-\frac{2\nu^{(f)}}{\nu^{(f)}-1}\alpha'^{(f)}T(r,z=0). \tag{33}$$

In the $W\to\infty$ limit, the elastic strain in the film at $r=0$ is obtained by using Eqs. (27):

$$\bar{\epsilon}^f_{rr}(r=0)=\bar{\epsilon}^f_{\theta\theta}(r=0)=\left(\frac{\nu^{(s)}+1}{2}\alpha'^{(s)}-\alpha'^{(f)}\right)T_{\max}, \tag{34a}$$

$$\bar{\epsilon}^f_{zz}(r=0)=\frac{2\nu^{(f)}}{\nu^{(f)}-1}\times\left(\frac{\nu^{(s)}+1}{2}\alpha'^{(s)}-\alpha'^{(f)}\right)T_{\max}. \tag{34b}$$

These equations for thin-film elastic strain at the origin during focused laser heating are evaluated now for two examples with $T_{\max}=1400$ K ($W=\infty$). (The built-in strains are still assumed to be zero.) For silicon films on sapphire, $\bar{\epsilon}_{rr}=\bar{\epsilon}_{\theta\theta}=+3.0\times10^{-4}$ and $\bar{\epsilon}_{zz}=-4.3\times10^{-4}$, using $\alpha'=8.6\times10^{-6}/°C$ and $\nu=-0.02$ for the sapphire substrate.[12] In this case, each elastic strain is of opposite sign from the respective component for a silicon substrate (or for a Si film on Si). These elastic strains are also much smaller in magnitude than those in silicon because of the near cancellation of the two terms in brackets in Eqs. (34). This near cancellation occurs whether coefficients of thermal expansion that have been averaged over temperature are used, as is done here, or coefficients at any given temperature from 300 to 1690 K are employed. For silicon thin films on fused silica (SiO_2), $\bar{\epsilon}_{rr}=\bar{\epsilon}_{\theta\theta}=-5.1\times10^{-3}$ and $\bar{\epsilon}_{zz}=+7.5\times10^{-3}$, using $\alpha'=5.5\times10^{-7}/°C$ and $\nu=0.17$ for fused silica.[12] These elastic strains are significantly larger than those in silicon substrates and have the same sign. The Si on SiO_2 case is not very sensitive to the variations of α' with temperature.

Murakami[17] has shown that the stress and strain distributions in large-diameter, thin-disk microstructures are quite uniform away from the disk edges. This suggests that this thin-film analysis can be extended to regions near the center of disk-type microstructures on substrates.

III. IMPLICATIONS OF STRESSES AND STRAINS IN LOCALIZED LASER HEATING

A. Stress-induced defect formation

Residual stresses induced during laser heating can produce defects that remain in the material after processing. For example, in crystalline silicon, stress in excess of the yield stress can induce dislocations on the {111} slip planes in the ⟨110⟩ slip directions.[18] If these dislocations are formed because of laser heating, then after heating they will be frozen. This leads to large built-in stresses near the defect, which can affect subsequent performance in microelectronics applications. Usually, these defects will not be annealed away during the later phases of laser heating. Dislocations formed in c-Si by laser-heating-induced stresses are analyzed here as a specific example.

Consider (100) Si with the x, y, and z axes chosen to be the [100], [010], and [001] directions, respectively. Since $\sigma_{\theta z}=0$ (and also $\sigma_{r\theta}=0$) by symmetry, and since σ_{rz} is so small that it is effectively zero, the off-diagonal stresses $\sigma_{yz}=\sigma_{xz}=0$. In c-Si there are three ⟨110⟩ slip directions on each of the four {111} slip planes. With these conditions there are five distinct ways to project stresses along the 12 combinations of slip directions on slip planes.[3] S_i are the magnitudes of these projected stresses:

$$S_1=\frac{1}{\sqrt{6}}\,|\sigma_{xx}-\sigma_{yy}|,$$

$$S_{2,3}=\frac{1}{\sqrt{6}}\,|\sigma_{xx}\pm\sigma_{xy}-\sigma_{zz}|, \tag{35}$$

$$S_{4,5}=\frac{1}{\sqrt{6}}\,|\sigma_{yy}\pm\sigma_{xy}-\sigma_{zz}|.$$

Dislocations are assumed to form at any position r, θ, and z for which any of these projected stresses exceed the yield stress σ_E.

These expressions can be related to the results of Sec. II by converting the stresses in Table I to Cartesian coordinates:

$$\sigma_{xx}=\frac{\sigma_{rr}+\sigma_{\theta\theta}}{2}+\frac{\sigma_{rr}-\sigma_{\theta\theta}}{2}\cos 2\theta,$$

$$\sigma_{xy}=\frac{\sigma_{rr}-\sigma_{\theta\theta}}{2}\sin 2\theta,$$

$$\sigma_{yy}=\frac{\sigma_{rr}+\sigma_{\theta\theta}}{2}-\frac{\sigma_{rr}-\sigma_{\theta\theta}}{2}\cos 2\theta,$$

$$\sigma_{zz}=\sigma_{zz}. \tag{36}$$

The projected stresses are then

$$S_1=\frac{1}{\sqrt{6}}\,|(\sigma_{rr}-\sigma_{\theta\theta})\cos 2\theta|,$$

$$S_{2\text{-}5}=\frac{1}{\sqrt{6}}\left|\frac{\sigma_{rr}+\sigma_{\theta\theta}}{2}-\sigma_{zz}+\frac{\sigma_{rr}-\sigma_{\theta\theta}}{\sqrt{2}}\sin\left(2\theta+\frac{m\pi}{4}\right)\right|, \tag{37}$$

where $m=0,1,2,$ and 3 correspond to S_5, S_3, S_2, and S_4, respectively.

It is important to determine the maximum projected stress $S^{\max}$ for comparison to the yield stress. For example, on the $r=0$ symmetry axis, $\sigma_{rr}=\sigma_{\theta\theta}$, and so

$$S_{2\text{-}5}^{\max}(r=0,\theta,z)=\frac{1}{\sqrt{6}}\left|\frac{\sigma_{rr}+\sigma_{\theta\theta}}{2}-\sigma_{zz}\right|,$$

while $S_1=0$. For $r=0$ and $z=0$ in the limit $W\to\infty$, $\sigma_{rr}=\sigma_{\theta\theta}=\sigma_{\max}$ and $\sigma_{zz}=0$ (because of the boundary condition imposed at $z=0$), and so $S_{2\text{-}5}^{\max}=\sigma_{\max}/\sqrt{6}$ in this limiting case.

More generally, S_1 reaches a maximum value of

$$S_1^{\max}(r,\theta,z)=\frac{1}{\sqrt{6}}\,(\sigma_{rr}-\sigma_{\theta\theta}) \tag{38}$$

at the four angles $\theta=m'(\pi/2)$ ($m'=0\text{–}3$) for each r and z. $S_{2\text{-}5}$ collectively reach maxima of

$$S_{2\text{-}5}^{\max}(r,\theta,z)=\frac{1}{\sqrt{6}}\left(\left|\frac{\sigma_{rr}+\sigma_{\theta\theta}}{2}-\sigma_{zz}\right|+\left|\frac{\sigma_{rr}-\sigma_{\theta\theta}}{\sqrt{2}}\right|\right) \tag{39}$$

at the eight angles $\theta=\pi/8+(m''\pi/4)$ ($m''=0\text{–}7$).

$S_1^{\max}$ and $S_{2\text{-}5}^{\max}$ are displayed in Fig. 7 for $W=15$, as a function of r for several values of z from 0 to 4 μm, using the plots of stress in Fig. 2. The maximum projected stress occurs on the surface for the $S_{2\text{-}5}$ slip plane/direction combinations. Although this projected stress actually peaks near 0.8 μm, it is still quite flat from the axis to the radius. The value

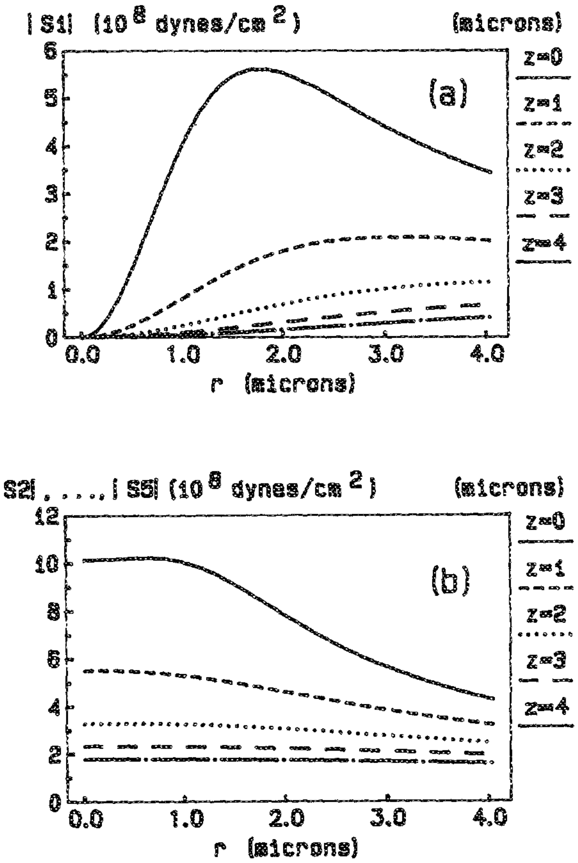

FIG. 7. Magnitude of maximum stresses in silicon projected on the {111} slip planes in the ⟨110⟩ directions using stresses from Fig. 2: (a) $S_1^{\max}$ and (b) $S_{2\text{-}5}^{\max}$.

on axis is slightly smaller than the $\sigma_{max}/\sqrt{6}$ value determined above the $W\to\infty$ limit, because $W=15$ in the numerical integration. The peak of S_1 occurs on the surface about 1.8 μm from the axis, where it is still smaller than the $S_{2\text{-}5}$ projected stress maxima. Therefore, the regions of maximum projected stress are at the surface, along the eight rays projecting from the origin to $r\approx 1$ μm, which correspond to the eight angles of $S_{2\text{-}5}^{max}$.

The yield stress σ_E of several materials depend on the rate of strain as[18]

$$\sigma_E = C_0\left(\frac{\partial|\bar{\epsilon}|}{\partial t}\right)^{1/n}\exp\left(\frac{U}{nk_BT_t}\right), \tag{40}$$

where U is the activation energy for glide movement, and C_0 and n are constants. For Si, $U=2.3$ eV, $n=2.1$, and $C_0=1.7\times10^5$ (dyn/cm^2)s$^{1/n}$.[18] The large W limit for the projected stress, $\sigma_{max}/\sqrt{6}$, will be used to ascertain the experimental conditions for which the maximum projected stress exceeds this yield stress during laser heating by a scanning Gaussian beam. If the scan speed of the laser is v, the dwell time of the laser over a distance of the spot size w is w/v. Therefore the elastic strain rate at the origin is $\partial|\bar{\epsilon}|/\partial t \approx (v/w)|\bar{\epsilon}|$. After projecting the elastic strain at the origin [as in Eqs. (37)] and using Eq. (40), the range of v/w where the maximum projected stress exceeds the yield stress is then obtained:

$$\frac{v}{w} < \frac{1}{\nu+1}\left(\frac{E}{C_0}\right)^n\left(\frac{\alpha' T_{max}}{2\sqrt{6}}\right)^{n-1}\exp\left(-\frac{U}{k_BT_t}\right). \tag{41}$$

The minimum permissable scanning speed with no dislocation formation is tabulated in Table III, using the parameters for silicon and spot size of $w=1$ μm, for various values of T_{max}. At relatively low peak laser-heated temperatures ($T_t<1090$ K), scan speeds can be quite slow ($\leqslant 1$ μm/s) without inducing defects. At higher temperatures, dislocations will form at these slow speeds, according to this model. When the laser heats the spots nearly to melting, defects will form at speeds slower than about 10 mm/s. This speed corresponds to the fastest demonstrated speeds for direct laser writing.[1] Consequently, this analysis suggests that surface damage may indeed occur in many operating regimes of laser writing on silicon substrates.

B. Strain effects on the Raman spectrum

Raman analysis can probe laser heating by examining the temperature-dependent phonon frequency shift, phonon linewidth, and/or scattering intensity. Of these three methods, measurement of frequency shifts and linewidths are usually the most reliable probes of temperature.[19] However, if the temperature varies significantly within the beam spot size of the Raman probe laser, the Raman spectrum will be a spatially averaged profile, which must be interpreted with care.[19]

Strains induced in laser heating will also perturb the Raman spectrum. The thermal component of the total strain is already included in the temperature dependence of the phonon frequency. Only the effect of deviations from thermal equilibrium of unstressed material, i.e., due to elastic strains $\bar{\epsilon}$, need therefore be considered separately in Raman analysis. The effect of strain in the Raman analysis of laser-heated silicon will be addressed here.

In c-Si the $k=0$ optical phonon near 520 cm^{-1} is triply degenerate. This degeneracy is at least partly lifted by nonhydrostatic stress. Following the treatment of Anastassakis *et al.*,[20] the phonon frequencies for this cubic material may be obtained from

$$\det\begin{vmatrix} p\bar{\epsilon}_{xx}+q(\bar{\epsilon}_{yy}+\bar{\epsilon}_{zz})-\bar{\lambda} & 2r\bar{\epsilon}_{xy} & 2r\bar{\epsilon}_{xz} \\ 2r\bar{\epsilon}_{xy} & p\bar{\epsilon}_{yy}+q(\bar{\epsilon}_{xx}+\bar{\epsilon}_{zz})-\bar{\lambda} & 2r\bar{\epsilon}_{yz} \\ 2r\bar{\epsilon}_{xz} & 2r\bar{\epsilon}_{yz} & p\bar{\epsilon}_{zz}+q(\bar{\epsilon}_{xx}+\bar{\epsilon}_{yy})-\bar{\lambda}\end{vmatrix}=0, \tag{42}$$

with $\bar{\lambda}=\omega^2-\omega_0^2$, where ω_0 is the unperturbed frequency at the given temperature T_t, and ω is the phonon frequency perturbed by the elastic strains $\bar{\epsilon}$.

If $\bar{\lambda}<\omega^2$ and ω_0^2, as is usually true, then $\omega\cong\omega_0+(\bar{\lambda}/2\omega_0)$. p, q, and r have been measured for c-Si at room temperature: $p=-1.43\times10^{28}/\text{s}^2$, $q=-1.89\times10^{28}/\text{s}^2$, and $r=-0.59\times10^{28}/\text{s}^2$.[21]

TABLE III. Minimum scan velocity with no dislocation formation in silicon for different maximum laser-heated temperatures, with $w=1$ μm in the limit $W\to\infty$.

T_{max} (K)	[T_t (K)]	v_{min} (μm/s)	
600	[890]	0.0031	
800	[1090]	1.0	
1000	[1290]	60	
1200	[1490]	1 200	(1.2 mm/s)
1400	[1690]	12 000	(12 mm/s)

The relations between the elastic strains derived here in cylindrical coordinates (Table I) and those in Cartesian coordinates are simplified because the temperature profile is cylindrically symmetric and therefore $\epsilon_{r\theta}=\epsilon_{\theta z}=0$. Also, the numerical integration presented in Sec. II has shown that $\epsilon_{rz}\ll\epsilon_{rr}$, $\epsilon_{\theta\theta}$, and ϵ_{zz}. Therefore, it is reasonable to set $\epsilon_{rz}=0$. This leads to

$$\begin{aligned}\bar{\epsilon}_{xx}&=(\cos^2\theta)\bar{\epsilon}_{rr}+(\sin^2\theta)\bar{\epsilon}_{\theta\theta},\\ \bar{\epsilon}_{xy}&=\sin\theta\cos\theta(\bar{\epsilon}_{rr}-\bar{\epsilon}_{\theta\theta}),\\ \bar{\epsilon}_{yy}&=(\sin^2\theta)\bar{\epsilon}_{rr}+(\cos^2\theta)\bar{\epsilon}_{\theta\theta},\\ \bar{\epsilon}_{zz}&=\bar{\epsilon}_{zz},\end{aligned} \tag{43}$$

with $\bar{\epsilon}_{yz}=\bar{\epsilon}_{xz}=0$. It should be remembered that since the thermoelastic analysis has assumed material isotropy and silicon has cubic symmetry, this treatment is only approximate.

On axis ($r=0$), $\epsilon_{rr}=\epsilon_{\theta\theta}$, and so $\bar{\epsilon}_{xx}=\bar{\epsilon}_{yy}$, which is expected from symmetry; also $\bar{\epsilon}_{xy}=0$. Therefore, on axis the triplet breaks up into a singlet and doublet with frequencies ω_s and ω_d, respectively. From Eq. (42),

$$\omega_s(r=0,z)=\omega_0+\frac{1}{2\omega_0}(2q\bar{\epsilon}_{rr}+p\bar{\epsilon}_{zz}), \quad (44a)$$

$$\omega_d(r=0,z)=\omega_0+\frac{1}{2\omega_0}[(p+q)\bar{\epsilon}_{rr}+q\bar{\epsilon}_{zz}]. \quad (44b)$$

More generally ($r\neq 0$), symmetry is lost totally and the triplet splits into three singlets: ω_1, ω_2, and ω_3, with ω_1 corresponding to the singlet ω_s in the above equation:

$$\omega_1(r,\theta,z)=\omega_0+\frac{1}{2\omega_0}[q(\bar{\epsilon}_{rr}+\bar{\epsilon}_{\theta\theta})+p\bar{\epsilon}_{zz}], \quad (45a)$$

$$\omega_{2,3}(r,\theta,z)=\omega_0+\frac{1}{2\omega_0}\left\{\frac{p+q}{2}(\bar{\epsilon}_{rr}+\bar{\epsilon}_{\theta\theta})+q\bar{\epsilon}_{zz}\pm(\bar{\epsilon}_{rr}-\bar{\epsilon}_{\theta\theta})\left[\left(\frac{p-q}{2}\cos(2\theta)\right)^2+[r\sin(2\theta)]^2\right]^{1/2}\right\}. \quad (45b)$$

In Eq. (45) there is an explicit dependence on r and z in the $\bar{\epsilon}$ terms, and an implicit dependence through the temperature dependence in ω_0 (and also through the possible temperature dependence of p, q, and r).

In addition to the variation of $\omega_{1,2,3}$ with r and z, which would be apparent during probing when induced strains are fairly uniform, there may be averaging effects (strain-induced broadening) when the probed region is not small compared to the spatial variations in $\bar{\epsilon}$. This is analogous to the possible spatial averaging in the temperature-induced Raman shift. For $\omega_{2,3}$ the Raman shift depends also on θ, varying as 2θ. In backscattering studies on (100)Si, the ω_1 (ω_s) Raman peak can be isolated by proper selection of polarization, and so this last spectral complication can be avoided.

For $T_{\max}=1400$ K ($T_t=1690$ K) the Raman shift modified by only temperature effects is about 480 cm^{-1},[22] downshifted by about 40 cm^{-1} from the shift at room temperature. For $r=0$ and $z=0$ in the $W\to\infty$ limit with $T(r=0,z=0)=T_{\max}=1400$ K, the singlet ω_1 is upshifted by 0.8 cm^{-1}, while the doublet $\omega_{2,3}$ is upshifted by only 0.3 cm^{-1} relative to 480 cm^{-1}. The local silicon optical phonon triplet frequencies for $T_{\max}=1400$ K and $W=15$, are displayed in Fig. 8 as a function of r and z at $\theta=0$. The $\omega_{2,3}$ phonon frequencies for $\theta=\pi/4$ (not shown) are near the frequencies for $\theta=0$. Exclusion of these elastic strain effects in the Raman measurement of temperature will lead to an underestimate of the temperature by only about 35 K, when the silicon is laser heated near 1600 K.

The values for the peak elastic-strain-induced Raman shifts in (100) silicon during Gaussian beam heating calculated here are smaller by roughly a factor of 5 vis-à-vis those given for more uniform laser heating in Refs. 4 and 5, for equal laser-heated peak temperatures. The analysis in these cited studies assumed that the laser induces a uniform two-dimensional compressive stress and may not have taken into account the effect of the zz component of elastic strain. $\bar{\epsilon}_{zz}$ is

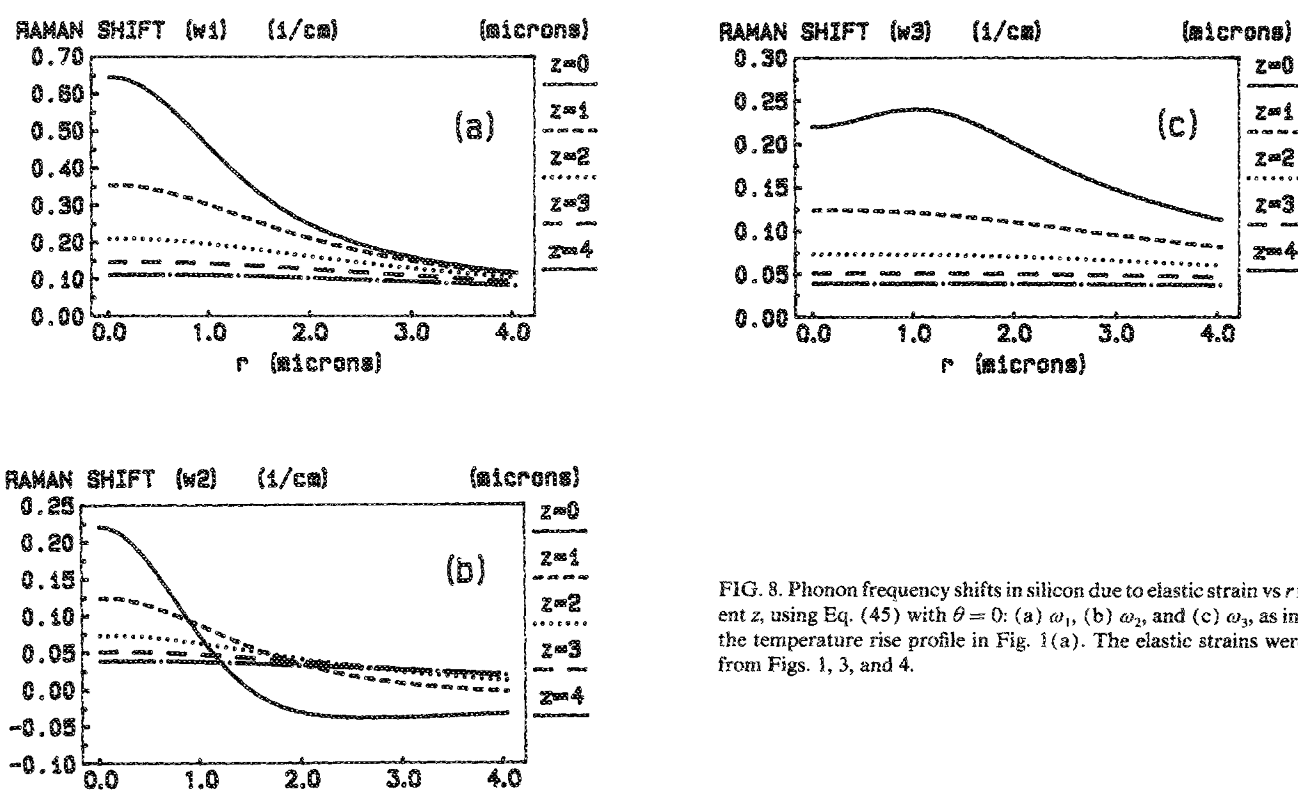

FIG. 8. Phonon frequency shifts in silicon due to elastic strain vs r for different z, using Eq. (45) with $\theta=0$: (a) ω_1, (b) ω_2, and (c) ω_3, as induced by the temperature rise profile in Fig. 1(a). The elastic strains were derived from Figs. 1, 3, and 4.

extremely important in Raman analysis. Exclusion of this zz component in Eqs. (44) and (45) leads to significantly larger strain-induced Raman shifts than when it is included properly.

The phonon shifts due to elastic strains induced during laser heating of thin films on substrates are now evaluated for the two cases examined in Sec. II B. As before, $T_{\max} = 1400$ K and $W = \infty$. For silicon films on sapphire, at $r = 0$ and $z = 0$ the singlet ω_1 is downshifted by 0.15 cm^{-1} and $\omega_{2,3}$ is downshifted by 0.05 cm^{-1}, relative to 480 cm^{-1}. For silicon thin films on fused silica (SiO_2), ω_1 and $\omega_{2,3}$ increase by 2.6 and 0.9 cm^{-1}, respectively. The effect of elastic strain is to increase the phonon frequencies for both silicon substrates and Si thin films on SiO_2, while it decreases the Raman shifts for a Si thin film atop a sapphire substrate. The shifts are quite small in magnitude for silicon on sapphire because of the small elastic strains induced in laser heating, as discussed in Sec. II B. In contrast, the magnitudes of the Raman shifts for silicon on SiO_2 are significantly larger than those for a Si substrate, and they are large enough to affect Raman microprobe determination of surface temperature significantly, leading to an underestimate of T by about 115 K for $T_{\max} = 1400$ K. Including built-in strains at the thin-film/substrate interface will modify these results.

Within the Raman probed volume, uniform elastic strains will shift the central frequency of the Raman profile, while strain nonuniformities will broaden the line shape. Strain can also change the Raman scattering intensity. Calculations by Wendel[23] have shown that in silicon, strain can increase the Raman scattering probability, particularly as the probe laser frequency approaches the direct band-gap frequency. Nonhydrostatic stresses can also alter the Raman polarization selection rules, by changing the local symmetry of the lattice.[4,24]

IV. CONCLUDING REMARKS

This paper has presented analytic expressions which are useful in analyzing the physical conditions during laser processing of materials, as in direct laser writing and laser annealing. With minor modifications this study can be used to investigate thermoelastic effects during heating by other sources, such as electron beams. Though the expressions given here are exact only for the stated conditions, e.g., temperature-independent parameters, isotropy, etc., they still provide very good estimates for more complicated experimental conditions.

Most of the results derived here are strictly valid only in the early stages of pyrolytic direct laser writing. For example, during laser deposition the temperature profile may change with time because the deposit may modify the optical and thermal conditions. Also, in some cases the stresses and strains occurring within the deposit during writing may prove to be more important in subsequent applications than those induced in the substrate; only the stresses and strains induced in the substrate, which may have a thin-film overlayer, were considered here. Furthermore, after deposition "built-in" stresses and strains may form at the deposit/substrate interface upon cooling, due to the different coefficients of thermal expansion in the deposit and substrate. These effects were not considered in this study.

The two examples discussed in Sec. III do, however, demonstrate the importance of considering thermoelastic effects in optical processing and diagnostics. Although the model used here for dislocation formation in silicon is only approximate, it does suggest that the stresses induced during laser processing may lead to undesirable consequences in applications using the processed material. Some optical properties of materials are indeed quite sensitive to strain. In Raman analysis of some silicon-based structures these laser-induced strains are not very important, as for silicon films on sapphire, but in some cases, such as silicon thin films on fused silica, these strains may affect the interpretation of the Raman data significantly.

ACKNOWLEDGMENT

This work was supported by the Office of Naval Research.

APPENDIX

The stress-strain relations including thermal expansion in cylindrical-coordinates are[25]

$$\sigma_{rr} = \frac{E\nu}{(1+\nu)(1-2\nu)}(\epsilon_{rr} + \epsilon_{\theta\theta} + \epsilon_{zz}) + \frac{E}{1+\nu}\epsilon_{rr} - \frac{E}{1-2\nu}\alpha' T, \tag{A1a}$$

$$\sigma_{\theta\theta} = \frac{E\nu}{(1+\nu)(1-2\nu)}(\epsilon_{rr} + \epsilon_{\theta\theta} + \epsilon_{zz}) + \frac{E}{1+\nu}\epsilon_{\theta\theta} - \frac{E}{1-2\nu}\alpha' T, \tag{A1b}$$

$$\sigma_{zz} = \frac{E\nu}{(1+\nu)(1-2\nu)}(\epsilon_{rr} + \epsilon_{\theta\theta} + \epsilon_{zz}) + \frac{E}{1+\nu}\epsilon_{zz} - \frac{E}{1-2\nu}\alpha' T, \tag{A1c}$$

$$\sigma_{rz} = \mu\epsilon_{rz}, \tag{A1d}$$

$$\sigma_{r\theta} = \mu\epsilon_{r\theta}, \tag{A1e}$$

$$\sigma_{z\theta} = \mu\epsilon_{z\theta}, \tag{A1f}$$

where E is Young's modulus, ν is Poisson's ratio, μ is the shear modulus, and α' is the coefficient of thermal expansion. σ is the residual stress, ϵ is the (total) strain, which is the sum of elastic and thermal strains, and T is the laser-induced temperature rise. For media with cubic symmetry, elastic constants are related to E, ν, and μ by

$$C_{12} = \frac{E\nu}{(1+\nu)(1-2\nu)},$$

$$C_{11} - C_{12} = \frac{E}{1+\nu},$$

$$C_{44} = \mu.$$

For the isotropic media considered here

$$C_{44} = \frac{1}{2}(C_{11} - C_{12}) = \mu = \frac{E}{2(1+\nu)}.$$

Total strains are defined in terms of total displacements u, as follows:

$$\epsilon_{rr} = \frac{\partial u_r}{\partial r}, \tag{A2a}$$

$$\epsilon_{\theta\theta} = \frac{1}{r}\frac{\partial u_\theta}{\partial \theta} + \frac{u_r}{r}, \tag{A2b}$$

$$\epsilon_{zz} = \frac{\partial u_z}{\partial z}, \tag{A2c}$$

$$\epsilon_{rz} = \frac{\partial u_z}{\partial r} + \frac{\partial u_r}{\partial z}, \tag{A2d}$$

$$\epsilon_{r\theta} = \frac{1}{r}\frac{\partial u_r}{\partial \theta} + \frac{\partial u_\theta}{\partial r} - \frac{u_\theta}{r}, \tag{A2e}$$

$$\epsilon_{\theta z} = \frac{\partial u_\theta}{\partial z} + \frac{1}{r}\frac{\partial u_z}{\partial \theta}. \tag{A2f}$$

At equilibrium with no external forces, the stresses are related by[25]

$$\frac{\partial \sigma_{rr}}{\partial r} + \frac{1}{r}\frac{\partial \sigma_{r\theta}}{\partial \theta} + \frac{\partial \sigma_{rz}}{\partial z} + \frac{\sigma_{rr} - \sigma_{\theta\theta}}{r} = 0, \tag{A3a}$$

$$\frac{\partial \sigma_{r\theta}}{\partial r} + \frac{1}{r}\frac{\partial \sigma_{\theta\theta}}{\partial \theta} + \frac{\partial \sigma_{\theta z}}{\partial z} + \frac{2}{r}\sigma_{r\theta} = 0, \tag{A3b}$$

$$\frac{\partial \sigma_{rz}}{\partial r} + \frac{1}{r}\frac{\partial \sigma_{\theta z}}{\partial \theta} + \frac{\partial \sigma_{zz}}{\partial z} + \frac{1}{r}\sigma_{rz} = 0. \tag{A3c}$$

Equations (A3a)–(A3c) are solved by first replacing the stresses by the strains from Eqs. (A1a)–(A1f) and then expressing the strains in terms of displacements, using Eqs. (A2a)–(A2f). One convenient way to proceed is to use Youngdahl stress functions[9] Ω, Ψ, and Λ in the resulting modified Eqs. (A3). These functions are related to displacements by

$$u_r = \frac{\partial \Omega}{\partial r} - \frac{1}{r}\frac{\partial \Lambda}{\partial \theta}, \tag{A4a}$$

$$u_\theta = \frac{1}{r}\frac{\partial \Omega}{\partial \theta} + \frac{\partial \Lambda}{\partial r}, \tag{A4b}$$

$$u_z = \frac{\partial \Omega}{\partial z} + \frac{\partial \Psi}{\partial z}. \tag{A4c}$$

Now, assuming an isotropic medium and an axisymmetric temperature profile, the stresses and strains are cylindrically symmetric and u_θ, $\epsilon_{\theta r}$, $\epsilon_{\theta z}$, $\sigma_{\theta r}$, $\sigma_{\theta z}$, and $\Lambda = 0$.

Then

$$u_r = \frac{\partial \Omega}{\partial r}, \tag{A4a$'$}$$

$$u_z = \frac{\partial \Omega}{\partial z} + \frac{\partial \Psi}{\partial z}, \tag{A4b$'$}$$

and

$$\epsilon_{rr} = \frac{\partial^2 \Omega}{\partial r^2}, \tag{A5a}$$

$$\epsilon_{\theta\theta} = \frac{1}{r}\frac{\partial \Omega}{\partial r}, \tag{A5b}$$

$$\epsilon_{zz} = \frac{\partial^2 \Omega}{\partial z^2} + \frac{\partial^2 \Psi}{\partial z^2}, \tag{A5c}$$

$$\epsilon_{rz} = 2\frac{\partial^2 \Omega}{\partial r \partial z} + \frac{\partial^2 \Psi}{\partial r \partial z}. \tag{A5d}$$

After some rearrangement and a single integration, the modified Eqs. (A3a) and (A3c) may be expressed in terms of the Ω and Ψ stress functions:

$$\nabla^2 \Omega = \frac{1}{2(1-\nu)}\left(-\frac{\partial^2 \Psi}{\partial z^2} + 2(1+\nu)\alpha' T\right), \tag{A6}$$

$$\nabla^2 \Psi = 0. \tag{A7}$$

[1] For example, see I. P. Herman, in *Photochemical Materials Processing*, edited by K. G. Ibbs and R. M. Osgood (Cambridge University Press, Cambridge, 1988); D. Bauerle, *Chemical Processing with Lasers* (Springer, Berlin, 1986); Y. Rytz-Froidevaux, R. P. Salathe, and H. H. Gilgen, Appl. Phys. A **37**, 121 (1985).
[2] L. Correra and G. G. Bentini, J. Appl. Phys. **54**, 4330 (1983).
[3] G. Bentini, L. Correra, and C. Donolato, J. Appl. Phys. **56**, 2922 (1984).
[4] G. E. Jellison, Jr. and R. G. Wood, Mater. Res. Soc. Symp. Proc. **23**, 153 (1984).
[5] A. Compaan, M. C. Lee, and G. J. Trott, Phys. Rev. B **32**, 6731 (1985).
[6] M. Lax, J. Appl. Phys. **48**, 3919 (1977).
[7] M. Lax, Appl. Phys. Lett. **33**, 786 (1978).
[8] M. A. Olmstead, N. M. Amer, S. Kohn, D. Fournier, and A. C. Boccara, Appl. Phys. A **32**, 141 (1983).
[9] C. K. Youngdahl, Int. J. Eng. Sci. **7**, 61 (1969).
[10] H. Metzger and F. R. Kessler, Z. Naturforsch. **25a**, 904 (1970).
[11] A. G. Beattie and J. E. Schirber, Phys. Rev. B **1**, 1548 (1970).
[12] Y. S. Touloukian, R. K. Kirby, R. E. Taylor, and T. Y. R. Lee, *Thermal Expansion, Nonmetallic Solids* (Plenum, New York, 1977).
[13] G. E. Jellison, Jr. and F. A. Modine, Appl. Phys. Lett. **41**, 180 (1982).
[14] J. E. Moody and R. H. Hendel, J. Appl. Phys. **53**, 4364 (1982).
[15] I. D. Calder and R. Sue, J. Appl. Phys. **53**, 7545 (1982).
[16] M. Yamada, K. Nambu, and K. Yamamoto, J. Appl. Phys. **57**, 965 (1985).
[17] M. Murakami, CRC Crit. Rev. Solid State Mater. Sci. **11**, 317 (1984); M. Murakami, Thin Solid Films **69**, 253 (1980).
[18] H. Siethoff and P. Haasen, in *Lattice Defects in Semiconductors*, edited by P. R. Hasiguti (University Press, Tokyo, 1968), p. 491.
[19] G. D. Pazionis, H. Tang, L. Ge, and I. P. Herman, Mater. Res. Soc. Symp. Proc. **101**, 113 (1988); G. D. Pazionis, H. Tang, and I. P. Herman J. Quantum Electron. (to be published).
[20] E. Anastassakis, A. Pinczuk, E. Burstein, F. H. Pollak, and M. Cardona, Solid State Commun. **8**, 133 (1970).
[21] M. Chandrasekhar, J. B. Renucci, and M. Cardona, Phys. Rev. B **17**, 1623 (1978).
[22] M. Balkanski, R. F. Wallis, and E. Haro, Phys. Rev. B **28**, 1928 (1983).
[23] H. Wendel, Solid State Commun. **31**, 423 (1979).
[24] M. Yamada, K. I. Yamazaki, H. Kotani, K. Yamamoto, and K. Abe, in *Laser and Electron-Beam Solid Interactions-MRS Proceedings Vol. 1*, edited by J. F. Gibbons, L. D. Hess, and T. W. Sigmon (Elsevier, New York, 1981), p. 503.
[25] I. S. Sokolnikoff, *Mathematical Theory of Elasticity* (McGraw-Hill, New York, 1956).